Int. J. Pharm. Investigation, 2026; 16(4):1642-1656.
https://www.jpionline.org

Original Article

Structure-Guided Virtual Screening and Molecular Dynamics Simulation of Selective Small-Molecule Inhibitors Targeting E3 Ubiquitin Ligase MDM2 in Breast Cancer

Tahani Bakhsh*

Department of Biological Sciences, College of Science, University of Jeddah, Jeddah, SAUDI ARABIA.

ABSTRACT

Background: MDM2 is an E3 ubiquitin ligase that suppresses p53, promotes its degradation, inhibits apoptosis, and drives uncontrolled cancer cell growth. Targeting the MDM2-p53 interaction is therefore a promising strategy for solid tumor therapy. **Objectives:** To identify selective small-molecule MDM2 inhibitors with potential therapeutic value in breast cancer. **Materials and Methods:** A structure-based virtual screening workflow was performed on the MCULE platform. Selected hits were assessed using PASS, cell line prediction, safety, pharmacokinetic, and ADMET analyses, followed by molecular dynamics simulations to evaluate complex stability. **Results:** Virtual screening identified promising MDM2-targeting compounds. Subsequent profiling highlighted two lead candidates with predicted cytotoxic activity, favorable drug-like properties, and stable binding within the MDM2 pocket. **Conclusion:** Two potential small-molecule MDM2 inhibitors were identified as promising lead compounds for restoring p53 activity and developing targeted breast cancer therapies.

Keywords: Docking studies, E3 ubiquitin ligase, MDM2 inhibitors, Molecular Simulation, Anticancer, Structure-based virtual screening.

Correspondence:
Dr. Tahani Bakhsh
Department of Biological Sciences, College of Science, University of Jeddah, Jeddah, SAUDI ARABIA.
Email: tabakh@uj.edu.sa; tahanibakhsh@hotmail.com

Received: 11-03-2026;
Revised: 22-05-2026;
Accepted: 03-07-2026.

INTRODUCTION

Cancers remain one of the leading causes of mortality worldwide, and the dysregulation of cellular signaling pathways plays a critical role in tumor initiation and progression. Among these pathways, the p53 tumor suppressor pathway is essential for maintaining genomic stability by regulating cell cycle arrest, apoptosis, and DNA repair mechanisms. The Murine Double Minute 2 (MDM2) protein is an E3 ubiquitin ligase that negatively regulates p53 by promoting its ubiquitination and subsequent proteasomal degradation (Borrero *et al.*, 2021; Sciot, 2021). MDM2 was initially derived from purified acentric chromosomes found in the cell line that had gone through spontaneous transformation 3T3DM by cloning. The reason behind cloning the genes present in these abnormal chromosomes, also known as double minutes, is that they are often the source of gene amplification, which may lead to cellular proliferation and tumorigenesis. Amplification of a genomic clone of MDM2 in rodent cells resulted in high tumorigenic potential in nude mice. This point of data hinted at the fact that MDM2 might be oncogenic (Wang *et al.*, 2024; Yu *et al.*, 2014). In parallel, researchers in another lab were isolating proteins that interacted with the p53 tumor suppressor protein, based on the assumption that such proteins might be capable of modulating p53 function. The MDM2 binds to p53 via its N-terminal domain leads to the formation of the MDM2, p53 complex. This causes the masking of the p53 transcription activation domain and finally leads to a decrease in the transcriptional activity of p53. As per the literature, MDM protein acts as oncoproteins, which is frequently overexpressed in a wide variety of human cancers, thus facilitating tumorigenesis (Zhu *et al.*, 2025). Additionally, MDM2's ring finger domain serves as an E3 ligase for p53, resulting in p53 ubiquitination. Ubiquitination is a kind of post-translational modification carried out by a cascade of E1, E2, and E3 enzymes, which mediate the linking of ubiquitin to the amino group of lysine residues of target or client proteins' side chains (Callis, 2014; Checler *et al.*, 2000; Hepowit *et al.*, 2022).

The overexpression of MDM2 disrupts p-53 mediated tumor suppression, allowing cancer cells to evade apoptosis and proliferate. Normally, levels of tumor suppressor p53 remain very low due to MDM promoting p53 ubiquitination and degradation (Russano *et al.*, 2025). The most widely researched link between MDM proteins and cancer is their capability to bind ubiquitinate and degrade p53 through 26s proteasome (Hepowit *et al.*, 2022). When cells face DNA damage, oxidative stress, or lack of oxygen,

DOI: 10.5530/ijpi.20260058

MDM proteins are suppressed and p53 starts to accumulate. This results in triggering various signaling cascades that in turn cause cell cycle halt, DNA fixing, and cell death (Abuetabh *et al*., 2022).

MDMs suppress p53 level and function through the following main mechanism: though directly binding to p53 through its N-terminal domains, MDM2 blocks the transcription of p53-responsive genes. Secondly, MDMs regulate p53 in a way that they have the ability to form a dimer and catalyze the degradation of p53 protein via ubiquitin dependent pathway. Furthermore, MDMs have the potential to lead to the p53 shuttling from the nucleus, thereby hindering the binding of p53 to its targeted genes. It also stated that MDM2 lowers p53 activity levels (Brown *et al*., 2026; Subhasree *et al*., 2013; Zhao *et al*., 2015). Later, it was shown that MDM2 overexpression inhibited the p53 mediated activation of a reporter gene containing the responsive element. A possible mechanism of MDM2 oncogenicity was therefore proposed: inactivation of the p53 tumor suppressor gene. Besides that, various research indicates that MDM proteins also work independently of p53 in various cellular functions such as where the cell is at cell cycle control, cell differentiation, and metabolism, which broadens the functions of proto-oncoproteins even more (Kung *et al*., 2022).

MDM2 itself has direct tumorigenic capacity supporting oncogenic behavior after overexpression. Additionally, different types of MDM2 mRNA splicing variants and post-translational modifications may alter the course of the disease. Investigations have revealed that 5.9% of breast cancer cases had MDM2 gene amplification, which was about 17 times higher than that of normal cells. P21, a downstream cell cycle protein kinase inhibitor of p53, can block the cell cycle progression, exerting an anti-cancer effect in breast cancer (Shamloo *et al*., 2019; Sun *et al*., 2023). Estrogen Receptor alpha (ER) is a nuclear receptor and an oncoprotein that is expressed in approximately 70% of breast cancers and strongly correlates with MDM2. ER positively regulates MDM2 expression via p53 independent pathway while MDM2 induces ubiquitination and degradation of ER by forming a protein complex with it. Upon chemotherapy, MDM2 is capable of functioning as an E3 ubiquitin ligase to induce apoptosis in breast cancer cells (Habara *et al*., 2022; Patel *et al*., 2022; Tecalco-Cruz *et al*., 2017). A decrement of KLF6 expression results in an increase in it and decrease in p53 indicating that this dysregulation in MDM2 pathways is additionally correlated with the reduced survival of HCC patients after surgery (Choudhary *et al*., 2013).

In view of the context, it creates considerable prevalence of malignancies resulting in high morbidity and mortality. Therefore, disrupting MDM2-p53 interaction becomes a vital therapeutic strategy. Various small-molecule inhibitors have been developed, exhibiting some limitations. RG7112 (Nutlin-3a Compound) and similar agents can cause MDM2 inactivation through apoptosis. Nutlin 3a is well documented to block MDM2 p53 binding, thereby enhancing p53-dependent programmed cell death in osteosarcoma (Psatha *et al*., 2023). In addition to targeting the p53 axis, modulation of associated oncogenic pathways, such as STAT signaling, heat shock proteins are found to be involved in protein folding and stress response pathways that support tumor cell survival. Similarly, Matrix Metalloproteinase-9 (MMP-9) contributes to tumor invasion and metastasis (Lang *et al*., 2019). Therefore, our study employed a computational *in silico* approach to uncover the potential small-molecule inhibitors of MDM2 via structure-based drug design. The investigation was conducted using a variety of characteristics, including pharmacokinetics, drug-likeliness aspects, lethality predictions, molecular interaction, and molecular dynamics. The MDM2 protein was chosen for the investigation, with its own inhibitor treated as a control compound. Surpassing these parameters enables the identification of the potent lead candidates.

MATERIALS AND METHODS

Obtaining and Preparing the Target Protein

Protein Data Bank (https://www.rcsb.org/) was utilized for retrieving our aimed protein 3LBL in the pdb format. The protein was prepared by removing unwanted obstacles and elongating the hydrogen bonds through the BIOVIA Discovery Studio Visualizer 2021 (Berman, 2023).

Structure-Based Virtual Screening of Small Molecules

The Mcule platform was utilized for screening of small compounds, which provides comprehensive curated molecules for computer-aided drug discovery. It's a combination of multiple approaches within a single platform, such as hit identification, ligand-based screening, structure-based screening, access to purchasable compounds, and many more, enabling exploration of chemical spaces (Kiss *et al*., 2012; Malik *et al*., 2019; Sait *et al*., 2019).

We have employed the hit-identification workflow available within the structure-based virtual screening module of the Mcule platform for retrieving potential small compound inhibitors. Under the workflow section, different parameters were applied. RO5 violation was set to 0 to 1 (Muteeb *et al*., 2022). Rest was minimized. In the diversity selection, a sampler was selected, and a default value was selected. This allows direct screening of extensive compound libraries against a predefined target protein. The three-dimensional pre-processed targeted protein was then uploaded to the Mcule platform, and docking studies were performed using the Autodock Vina-enabled Mcule screening platform. The complex dimensions were used for grid box values (Alsamghan *et al*., 2020; Malik *et al*., 2019; Trott *et al*., 2010; Roskoski, 2023).

Inhibitor Docking Assessment

Additionally, the inhibitor compound (Control) docking was also conducted. 1-Click docking under lead optimization was utilized within the same Mcule platform. The inhibitor compound was downloaded from the protein data bank attached to the protein. This compound was then uploaded to 1-click docking, and the prepared target protein was loaded. Similarly, the binding dimensions were pasted and retrieved from the macromolecule complex. The results were generated based on different poses. Among those, the best pose having the highest docking score was selected and downloaded.

Structure-Based Toxicity Filtration

The generated small compounds were further tested for toxicity check based on the compounds' structure. The toxicity was also checked using Toxicity checker within the integrated Mcule platform (Kiss *et al*., 2012). All the compounds were checked individually by simply clicking on compounds ID and click for toxicity checker. These results will be displayed as PASS or FAIL, indicating compound toxicity and non-toxicity. This lead in sorting the filtering of the compounds.

Biological Activity Spectra Prediction

The biological activity spectrum was conducted to focus on the biologically active substances. For that, the online software PASS (prediction of activity spectra for substances) was utilized, which is widely used to predict more than 300 pharmacological properties based on the structure SMILES (Parasuraman, 2011). The SMILES generated from the Mcule platform were copied and pasted one by one. The results were generated with pa (probability of activity) and pi (probability of inactivity) values. The desired properties related to MDM2 were selected and retrieved. Compounds with higher Pa values compared to Pi values were also focused.

Study of Cancerous Cell Line Activity

The compound's potential to act against cancer was forecasted by use of the online server CLC-Pred. its capable of determining cytotoxic effects of chemical compounds against different human cancer cell lines on the basis of the structure similarity of anticancer agents already known. For that, the SMILES were again pasted on the server. The results were generated with probabilities of compound activity and inactivity against different cell lines. Additionally, in this IAP values were also generated (Inferred Antitumor Activity Probability), indicating the likelihood that the compound may exhibit. The greater the value, the more promising the potential will be (Bishwakarma *et al*., 2026; Cheng *et al*., 2024; Lagunin *et al*., 2023).

Prediction of Compounds Lethality

The online server GUSAR (http://www.way2drug.com/gusar/acutoxpredict.htmL) incorporated within the way2drug platform was used to predict acute rat toxicity. It presents the median LD_{50} values for different routes of administration, including oral, intravenous, intraperitoneal, and subcutaneous. They were also assigned to different classes according to the toxicity classification system (Zakharov *et al*., 2012).

Side Effects Profiling Assessment

The possible side effects were predicted using the online server ADVER-PRED (http://www.way2drug.com/adverpred/). The server predicts the side effects based on structure similarity, trained on known drug safety data, enabling early identification of potential safety risks (Ivanov *et al*., 2018).

Pharmacokinetics Profiling

The pharmacokinetic properties of the compounds were analyzed through the pkCSM server. The tool is widely utilized for predicting the ADMET (Absorption, Distribution, Metabolism, Excretion, and Toxicity) parameters, including absorption, distribution, metabolism, excretion, and toxicity. Parameters such as intestinal absorption, blood-brain barrier permeability, cytochrome P450 interactions, and total clearances can also be assessed in this to evaluate the drug-like properties and physiological behavior of the compounds. To that end, Deep-Pk, the extended version of pkCSM, was also used to examine additional features, such as biocontamination and environmental factors. SMILES were respectively used to check all these druggable features contributing to understanding the systemic exposure and stability of compounds in biological systems (Bultum *et al*., 2022; Pires *et al*., 2015).

Profiling of Simulation Studies

Molecular dynamics simulations are used to capture the movement of the atoms in a system. Therefore, as per the integrated analyses of all the parameters, the best compounds were selected to check for stability. There are different parameters in simulation studies for depicting the investigations such as RMSF (Root Mean Square Fluctuation), RMSD (Root Mean Square Deviation), Solvent surface area, radius of gyration, and hydrogen bonds. The dynamics simulation took place at 300 k by utilizing the GROMACS software with version 5.1.2. Afterward, complexes and topologies were created using the gmx grep of the GROMACS package. The forcefield CGenFF (CHARMm general force field) was then applied. The complexes were solvated using the TIP3 cubic box model. The next step was to neutralize the charges by adding salt after the boundary conditions (Khan *et al*., 2022; Saxena, 2019). With 25,000,000 steps, the steepest descent algorithm was utilized for minimizing the energy. With constant volume of temperature and pressure conditions (NVT and NPT), the temperature was set. At last, the mesh was generated using the Ewald method, and the simulation was set to perform at 100ns to gain deeper insights. Every individual parameter was considered

and analyzed carefully to obtain the refined compounds (Noumi *et al*., 2025; Petersen, 1995; Rahmati *et al*., 2025).

RESULTS

Screening of small molecules

A total of 100 molecules were generated along with Lipinski violations. The docking studies revealed binding energies ranging from -11.1 kcal/mol to -8.4 kcal/mol. All 100 molecules were tested for structural toxicity. The toxicity checker within the Mcule platform revealed 38 safer compounds in terms of structure. However, the inhibitor compound revealed toxicity with -7.8 kcal/mol binding energy, proving the compounds are better. The safer compounds with their binding energies and violations are listed in Table 1. The smiles of these compounds were extracted and saved for further parameterization.

Assessing Biological Activity Parameters

The biological activity spectra of the compounds were predicted using the online software PASS prediction. The results in Table 2 revealed the compounds showing different probability scores against parameters. The activities related to MDM2 were focused on selecting parameters such as antineoplastic, Transcription Factor STAT inhibitors, MMP9 (Extracellular Matrix Modulation), and heat shock protein inhibitors, along with the control (Bhatia *et al*., 2023; Camps-Fajol *et al*., 2025; Wolosowicz *et al*., 2025). A total of 10 compounds with 0 violations have been opted out for investigating several different parameters. The results were analyzed based on the probability of being active and inactive.

The series demonstrated that the control compound exhibited a high confidence score only in general antineoplastic activity but lacked other targets such as STAT3 or MMP9. The MCULE-9270762767 emerged as a promising inhibitor for STAT3 inhibitors, having the favorable pa>pi values. Also showing favorable values for other inhibitors, as well as lacking HSP-90 activity. Furthermore, MCULE-4592638188 was also identified as a potential HSP27 antagonist, supporting other parameters as well. However, the antineoplastic activity was not found. The other compound, MCULE-8527570511, displayed a balanced profile with moderate STAT inhibition and the highest antineoplastic potential among the tested compounds, showing that it belongs to the class of anti-cancer agents as well.

Prediction of Cell Lines

The computational analysis of cell line cytotoxicity provides a correlation between predicted molecular targets and specific cancer types. Among the multiple cancerous cell lines, only those that are related to the MDM2 axis were selected. Cell lines such as breast and lung carcinomas significantly overexpressed the MDM2 or amplified gene alongside p53. The abnormal elevation results in excessive degradation of p53, leading to the inability

Table 1: Docking scores with RO5 violations of filtered compounds.

MCULE ID	Docking score	RO5 violations
MCULE-6681529935-0-134	-10.1	1
MCULE-6464780543-0-172	-9.9	1
MCULE-9772505960-0-245	-9.8	1
MCULE-8883993037-0-266	-9.7	1
MCULE-7263785423-0-231	-9.5	1
MCULE-8615044604-0-132	-9.4	1
MCULE-3030350691-0-213	-9.4	1
MCULE-3437839167-0-295	-9.3	0
MCULE-1436369022-0-215	-9.3	1
MCULE-8454446844-0-136	-9.3	1
MCULE-4058053946-0-211	-9.3	0
MCULE-7331047671-0-140	-9.3	1
MCULE-2446676144-0-221	-9.2	1
MCULE-3340241418-0-122	-9.2	1
MCULE-7324342249-0-67	-9.2	1
MCULE-8554429594-0-215	-9.2	1
MCULE-2250129412-0-224	-9.2	1
MCULE-8527570511-0-144	-9.1	1
MCULE-7816669746-0-213	-9.1	1
MCULE-1116419285-0-129	-9	1
MCULE-7950646640-0-209	-8.8	1
MCULE-3528442415-0-272	-8.8	1
MCULE-5174431551-0-247	-8.7	0
MCULE-7895890639-0-176	-8.7	1
MCULE-1387096425-0-286	-8.7	1
MCULE-9377071399-0-227	-8.7	1
MCULE-9968692477-0-141	-8.7	1
MCULE-8263048398-0-238	-8.6	0
MCULE-1672373270-0-176	-8.6	1
MCULE-6928036014-0-245	-8.6	1
MCULE-9247823479-0-203	-8.5	1
MCULE-6647072513-0-199	-8.5	0
MCULE-7966990722-0-154	-8.4	1
MCULE-4407680809-0-181	-8.4	0
MCULE-5556268030-0-163	-8.4	0
MCULE-4592638188-0-189	-8.4	0
MCULE-9270762767-0-241	-8.4	0
MCULE-7383585135 -Mi-63*	-7.8	2

* Mi-63 is a reference molecule. Scores are presented in kcal/mol.

Table 2: PASS Prediction Parameters.

Compounds	TF STAT3 inhibitor		TF STAT inhibitor		HSP-27 antagonist		HSP-90 antagonist		Antineoplastic		MMP9 Expr. inhibitor	
	Pa	Pi	Pa	Pi	Pa	Pi	Pa	Pi	Pa	Pi	Pa	Pi
MCULE-3437839167-0-295	0,439	0,026	0,479	0,025	0,295	0,231	NA	NA	0,105	0,065	0,220	0,178
MCULE-4058053946-0-211	0,539	0,013	0,507	0,019	NA	NA	NA	NA	NA	NA	NA	NA
MCULE-5174431551-0-247	0,267	0,084	0,232	0,119	0,336	0,149	NA	NA	0,244	0,017	0,686	0,008
MCULE-8263048398-0-238	NA	NA	0,179	0,171	NA	NA	0,078	0,070	NA	NA	NA	NA
MCULE-6647072513-0-199	NA	NA	NA	NA	NA	NA	NA	NA	NA	NA	NA	NA
MCULE-4407680809-0-181	0,457	0,023	0,436	0,036	NA	NA	NA	NA	NA	NA	NA	NA
MCULE-5556268030-0-163	NA	NA	NA	NA	NA	NA	0,093	0,051	NA	NA	NA	NA
MCULE-4592638188-0-189	0,485	0,020	0,458	0,030	0,607	0,005	0,107	0,037	NA	NA	0,231	0,164
MCULE-9270762767-0-241	0,592	0,008	0,563	0,010	0,393	0,071	NA	NA	0,201	0,056	0,279	0,117
MCULE-8527570511-0-144	0,488	0,019	0,515	0,018	NA	NA	NA	NA	0,370	0,116	NA	NA
Control	NA	NA	NA	NA	NA	NA	NA	NA	0,737	0,020	NA	NA

NA: Not Applicable, Pa: Probability of Activity, and Pi: Probability of Inactivity; Comma (,) is used as a decimal separator (e.g., 0,488 =0.488).

to trigger apoptosis (Di Grazia *et al*., 2025; Hou *et al*., 2019). Similarly, it confers resistance to conventional treatments in lung cancer. The other cell line of leukemia was also focused on solid tumors like the lung and breast (Mirabelli *et al*., 2019; Whiteley *et al*., 2021). Likewise, other cell lines are also focused on. A detailed cell line type is mentioned for the chosen compounds in Table 3.

The compounds are renamed in numeric form from MCULE IDs. From the table, it has been observed that the control inhibitor compound maintained a high-confidence activity profile against leukemia and colorectal models, lacking the targeting characteristics more often. Whereas, the tested compounds exhibited a refined profile for solid tumor lineages with the exceeding IAP values of 0.8, reinforcing robustness, especially in the fields of lung and breast cancers. Interestingly, the highest IAP values for lung cancer and more breast cell lines were demonstrated by compound 8, whereas compound 10 showed the highest IAP values, especially in breast cancer type, suggesting the reliability of addressing p53-mediated degradation in these specific malignancies.

Acute Rat Toxicity Analysis

The toxicity profile of the lead candidates was further scrutinized through quantitative-structure activity relationship. The evaluation was done on the basis of acute toxicity (LD_{50}) across different administrative routes to determine if the compounds fall within the Applicable Domain (AD) to ensure reliability (Gadaleta *et al*., 2019; Zwickl *et al*., 2022). Every route was determined in mmol/kg, mg/kg, and with class shown in Table 4.

The table revealed that compounds possess a significant safety margin as compared to control one. All the compound showed higher values indicating higher dosage threshold before toxicity occurs. Whereas, most of the predictions including control falls into class IV and V which are characterized as low-toxicity categories.

Safety Profile Assessment

To assess the safety profile of the compounds, the possible side effects were predicted using the Adver-Pred server. The investigation evaluates the likelihood of compound based on its structural features by employing the Pa and Pi scores to ensure data reliability (Table 5).

The analysis revealed that the compounds maintained favorable safety profile. The primary concern identified across all compounds was hepatotoxicity. However, it was also noticed that compound 10 significantly showed lower probabilities exhibiting only 1 side effect. However, there are some compounds which also showed 2-3 side effects. Whereas, no side was observed for compound 2. The results indicate some possible side effects through which preventive steps could be taken.

Drug-likeness Profiling

The pharmacokinetics properties of the candidates were evaluated to determine ADMET (Absorption Distribution, Metabolism, excretion and Toxicity) parameter. Table 6 provides a detailed comparative assessment among the compounds along with the control compound across key physiological parameters.

The analysis revealed maintenance of high human intestinal absorption levels, improving membrane permeability. The clearance parameter possesses reduce need for frequent dosing, lacking control, balanced by the BBB penetration potential. Majorly, compounds also showed non-mutagenic status. Additional analysis by the Deep-Pk predicted highly safe biodegradation and Avian highly safe-medium profile supporting compounds, environment-friendly (Sadia *et al*., 2024). Therefore, the compounds represent an overall safety window.

Table 3: Probability Score of Various Cancerous Cell Lines.

Compounds	Pa	Pi	Cell-line	Description	Tissue/Organ	Type	IAP*
Control	0.646	0.004	RS4-11	Adult B acute lymphoblastic leukemia	Bone Marrow	Leukemia	0.835
	0.472	0.009	SW480	Colon adenocarcinoma	Colon	Adenocarcinoma	0.932
	0.457	0.001	SJSA-1	Osteosarcoma	Bone	Sarcoma	0.94
	0.396	0.05	HCT-116	Colon carcinoma	Colon	Carcinoma	0.89
	0.35	0.023	HCC1954	Breast Carcinoma	Breast	Carcinoma	0.829
	0.266	0.179	CL97	Lung adenocarcinoma	Lung	Adenocarcinoma	0.872
	0.207	0.205	MDA-MB-361	Breast adenocarcinoma	Breast	Adenocarcinoma	0.872
	0.118	0.102	NCI-H128	Small cell lung cancer	Lung	Carcinoma	0.908
1	0.365	0.078	MDA-MB-231	Breast adenocarcinoma	Breast	Adenocarcinoma	0.881
	0.359	0.076	COR-L23	Lung large cell carcinoma	Lung	Carcinoma	0.834
	0.312	0.094	HCC1954	Breast Carcinoma	Breast	Carcinoma	0.829
	0.292	0.024	MDA-MB-453	Breast adenocarcinoma	Breast	Adenocarcinoma	0.888
	0.238	0.074	RKO	Colon carcinoma	Colon	Carcinoma	0.879
	0.209	0.009	HOS-TE85	Osteosarcoma	Bone	Sarcoma	0.844
	0.206	0.13	MDA-MB-468	Breast adenocarcinoma	Breast	Adenocarcinoma	0.898
	0.144	0.076	SJSA-1	Osteosarcoma	Bone	Sarcoma	0.94
	0.132	0.094	T47D	Breast carcinoma	Breast	Carcinoma	0.936
	0.111	0.022	GHOSTCXCR4	Osteosarcoma	Bone	Sarcoma	1
2	0.508	0.006	COR-L23	Lung large cell carcinoma	Lung	Carcinoma	0.834
	0.329	0.048	HT	Lymphoma	Haematopoietic and lymphoid tissue	Leukemia	0.857
	0.308	0.103	HCC1954	Breast Carcinoma	Breast	Carcinoma	0.829
	0.251	0.065	U2OS	Osteosarcoma	Bone	Sarcoma	0.885
	0.248	0.094	MDA-MB-468	Breast adenocarcinoma	Breast	Adenocarcinoma	0.898
	0.174	0.036	NCI-H1993	Non-small cell lung cancer	Lung	Adenocarcinoma	0.913
	0.133	0.122	LoVo	Colon adenocarcinoma	Colon	Adenocarcinoma	0.911
3	0.674	0.006	NCI-H460	Non-small cell lung carcinoma	Lung	Carcinoma	0.906
	0.579	0.018	HT-29	Colon adenocarcinoma	Colon	Adenocarcinoma	0.888
	0.324	0.191	MCF7	Breast carcinoma	Breast	Carcinoma	0.836
	0.322	0.045	CL1-0	Lung adenocarcinoma	Lung	Adenocarcinoma	0.83
	0.31	0.017	MDA-MB-453	Breast adenocarcinoma	Breast	Adenocarcinoma	0.888
	0.276	0.109	K562	Erythroleukemia	Haematopoietic and lymphoid tissue	Leukemia	0.892
	0.214	0.071	HEL	Erythroleukemia	Blood	Leukemia	0.903
	0.182	0.096	LS174T	Colon adencocarcinoma	Colon	Adenocarcinoma	0.91
	0.151	0.055	HOS-TE85	Osteosarcoma	Bone	Sarcoma	0.844
	0.148	0.096	Caco-2	Colon adenocarcinoma	Colon	Adenocarcinoma	0.898
	0.106	0.097	143B	Osteosarcoma	Bone	Osteosarcoma	0.931
	0.105	0.044	LXFL529	Lung non-small cell carcinoma	Lung	Carcinoma	0.979
	0.098	0.022	MAXF401	Breast carcinoma	Breast	Carcinoma	0.983
	0.031	0.019	H322	Lung carcinoma	Lung	Carcinoma	1
	0.024	0.008	MCF7R	Breast carcinoma	Breast	Carcinoma	0.996
	0.012	0.008	Lu1	Lung carcinoma	Lung	Carcinoma	0.995

Compounds	Pa	Pi	Cell-line	Description	Tissue/Organ	Type	IAP*
	0.011	0.004	Col2	Colon carcinoma	Colon	Carcinoma	1
4	0.285	0.014	NCI-H1299	Non-small cell lung carcinoma	Lung	Carcinoma	0.916
	0.265	0.236	MCF7	Breast carcinoma	Breast	Carcinoma	0.836
	0.233	0.166	MDA-MB-231	Breast adenocarcinoma	Breast	Adenocarcinoma	0.881
5	0.923	0.003	HCC2998	Colon adenocarcinoma	Colon	Adenocarcinoma	0.872
	0.923	0.003	NCI-H226	Non-small cell lung carcinoma	Lung	Carcinoma	0.88
	0.914	0.003	NCI-H322M	Non-small cell lung carcinoma	Lung	Carcinoma	0.881
	0.902	0.004	NCI-H522	Non-small cell lung carcinoma	Lung	Carcinoma	0.877
	0.893	0.005	HCT-116	Colon carcinoma	Colon	Carcinoma	0.89
	0.888	0.004	KM12	Colon adenocarcinoma	Colon	Adenocarcinoma	0.875
	0.788	0.004	MDA-MB-468	Breast adenocarcinoma	Breast	Adenocarcinoma	0.898
	0.763	0.004	NCI-H23	Non-small cell lung carcinoma	Lung	Carcinoma	0.883
	0.753	0.005	OVCAR-3	Ovarian adenocarcinoma	Ovarium	Adenocarcinoma	0.907
	0.733	0.004	HOP-62	Non-small cell lung carcinoma	Lung	Carcinoma	0.898
	0.61	0.02	MDA-MB-231	Breast adenocarcinoma	Breast	Adenocarcinoma	0.881
	0.51	0.018	NCI-H460	Non-small cell lung carcinoma	Lung	Carcinoma	0.906
	0.43	0.007	U2OS	Osteosarcoma	Bone	Sarcoma	0.885
	0.291	0.106	HT-29	Colon adenocarcinoma	Colon	Adenocarcinoma	0.888
	0.274	0.112	C8166	Leukemic T-cells	Blood	Leukemia	0.839
	0.135	0.115	HOS-TE85	Osteosarcoma	Bone	Sarcoma	0.844
6	0.333	0.219	DU-4475	Breast Carcinoma	Breast	Carcinoma	0.802
	0.291	0.059	NCI-H1581	Non Small Cell Lung Cancer	Lung	Carcinoma	0.871
	0.191	0.026	LoVo	Colon adenocarcinoma	Colon	Adenocarcinoma	0.911
	0.186	0.028	NCI-H2228	Non-small cell lung cancer	Lung	Adenocarcinoma	0.92
	0.146	0.035	PC-9	Lung adenocarcinoma	Lung	Adenocarcinoma	0.951
	0.143	0.078	SJSA-1	Osteosarcoma	Bone	Sarcoma	0.94
	0.032	0.019	HCC78	Lung adenocarcinoma	Lung	Adenocarcinoma	0.989
7	0.312	0.01	NCI-H1299	Non-small cell lung carcinoma	Lung	Carcinoma	0.916
	0.273	0.132	MDA-MB-231	Breast adenocarcinoma	Breast	Adenocarcinoma	0.881
	0.214	0.198	HOP-92	Non-small cell lung carcinoma	Lung	Carcinoma	0.862
	0.147	0.063	SJSA-1	Osteosarcoma	Bone	Sarcoma	0.94
8	0.375	0.055	COR-L23	Lung large cell carcinoma	Lung	Carcinoma	0.834
	0.373	0.149	DU-4475	Breast Carcinoma	Breast	Carcinoma	0.802
	0.37	0.144	HCC1937	Breast Carcinoma	Breast	Carcinoma	0.806
	0.344	0.038	NCI-H661	Lung carcinoma	Lung	Carcinoma	0.831
	0.336	0.134	CAL-51	Breast carcinoma	Breast	Carcinoma	0.824
	0.316	0.126	DMS-114	Lung carcinoma	Lung	Carcinoma	0.834
	0.303	0.151	RS4-11	Adult B acute lymphoblastic leukemia	Bone Marrow	Leukemia	0.835
	0.294	0.131	CL97	Lung adenocarcinoma	Lung	Adenocarcinoma	0.872
	0.285	0.094	HOS	Osteosarcoma	Bone	Sarcoma	0.863
	0.281	0.187	HCC1954	Breast Carcinoma	Breast	Carcinoma	0.829
	0.265	0.109	HCT-116	Colon carcinoma	Colon	Carcinoma	0.89
	0.262	0.165	NCI-H1703	Non Small Cell Lung Cancer	Lung	Carcinoma	0.851
	0.256	0.114	NCI-H1581	Non Small Cell Lung Cancer	Lung	Carcinoma	0.871

Compounds	Pa	Pi	Cell-line	Description	Tissue/Organ	Type	IAP*
	0.254	0.052	MDA-MB-453	Breast adenocarcinoma	Breast	Adenocarcinoma	0.888
	0.248	0.132	CL1-0	Lung adenocarcinoma	Lung	Adenocarcinoma	0.83
	0.242	0.099	MDA-MB-361	Breast adenocarcinoma	Breast	Adenocarcinoma	0.872
	0.226	0.111	MDA-MB-468	Breast adenocarcinoma	Breast	Adenocarcinoma	0.898
	0.225	0.096	U2OS	Osteosarcoma	Bone	Sarcoma	0.885
	0.213	0.133	RKO	Colon carcinoma	Colon	Carcinoma	0.879
	0.21	0.125	HOP-18	Non-small cell lung carcinoma	Lung	Carcinoma	0.933
	0.206	0.02	LoVo	Colon adenocarcinoma	Colon	Adenocarcinoma	0.911
	0.203	0.034	SK-BR-3	Breast adenocarcinoma	Breast	Adenocarcinoma	0.95
	0.164	0.143	LS174T	Colon adencocarcinoma	Colon	Adenocarcinoma	0.91
	0.157	0.031	SJSA-1	Osteosarcoma	Bone	Sarcoma	0.94
	0.133	0.024	143B	Osteosarcoma	Bone	Osteosarcoma	0.931
	0.091	0.025	NCI-H2286	Small cell lung cancer	Lung	Adenocarcinoma	0.968
	0.088	0.007	HEY	Ovarian carcinoma	Ovarium	Carcinoma	0.967
	0.045	0.007	H322	Lung carcinoma	Lung	Carcinoma	1
	0.024	0.017	C180-13S	Ovarian carcinoma	Ovarium	Carcinoma	0.999
9	0.377	0.013	U2OS	Osteosarcoma	Bone	Sarcoma	0.885
	0.377	0.038	HEK293	Embryonic kidney fibroblast	Kidney	Normal	0.898
	0.361	0.022	NCI-H661	Lung carcinoma	Lung	Carcinoma	0.831
	0.309	0.056	NCI-H1703	Non Small Cell Lung Cancer	Lung	Carcinoma	0.851
	0.226	0.176	CL1-0	Lung adenocarcinoma	Lung	Adenocarcinoma	0.83
	0.177	0.169	HOP-18	Non-small cell lung carcinoma	Lung	Carcinoma	0.933
	0.158	0.041	HOS-TE85	Osteosarcoma	Bone	Sarcoma	0.844
	0.131	0.128	LoVo	Colon adenocarcinoma	Colon	Adenocarcinoma	0.911
	0.079	0.043	NCI-H2286	Small cell lung cancer	Lung	Adenocarcinoma	0.968
10	0.488	0.013	MDA-MB-468	Breast adenocarcinoma	Breast	Adenocarcinoma	0.898
	0.279	0.087	NCI-H522	Non-small cell lung carcinoma	Lung	Carcinoma	0.877
	0.235	0.076	MDA-MB-453	Breast adenocarcinoma	Breast	Adenocarcinoma	0.888
	0.105	0.008	NCI-H2171	Small cell lung cancer	Lung	Carcinoma	0.953
	0.753	0.005	MOLT-4	Acute T-lymphoblastic leukemia	Blood	Leukemia	0.885

*IAP: Invariant Accuracy of Prediction.

Overall, the integrative analysis highlights the selection of final top compounds 8 and 10 as candidates for simulation studies. The combined analysis provides multidimensional validation. The data revealed that these compounds demonstrated the refined potential as STAT3, HSP-27, and MMP-9 inhibitors, showing the broad spectrum of cell lines against lung and breast carcinomas. They also represented higher LD_{50} values, outperforming the control in the safety panel. They also predicted reduced hepatotoxicity, enhanced pharmacokinetics profiling, and a non-mutagenic status of AMES with lower systemic clearance. Therefore, these compounds were selected to check for further simulation studies. The interacting diagram of these compounds, along with the control has illustrated in Figures 1A-C.

The figure showed representations of different poses of compounds, including an inhibitor compound. Different interacting bonds have been observed in a 2D diagram, such as van der Waals interaction, conventional hydrogen bonds, Pi alkyl, alkyl, Pi sigma, carbon hydrogen bonds, and halogen interactions. Interestingly, the interaction diagram showed most of the common residues of inhibitors found in both compounds. The commonly residues are noted as PHE55, VAL93, LEU54, VAL75, GLY58, ILE61, PHE91, ILE99, MET62, TYR67, ILE103, PHE86, LEU57, and ILE19. However, some additional residues, TYR100, MET17, and HIS96, are also observed in compound 10 from the reference inhibitor. This indicates a strong interacting profile of the compounds and support the findings.

Simulation Studies

To evaluate the stability of the compound and the binding persistence of the selected lead candidates within active sites, a simulation was performed at 100 ns. The analysis provides atomistic insights into the structural integrity of the protein-ligand complex. To depict the results, plots of RMSF, RMSD, SASA, Solvation, and Rg were generated.

Predicting Stability and flexibility (RMSD and RMSF)

The structural stability of complexes was analyzed through RMSD throughout the simulation (Maruyama *et al.*, 2023). The plot revealed that the reference molecule exhibited significant fluctuations ranging between 0.20 nm and 1.40 nm, particularly during approx. 60 ns, suggesting instability throughout the trajectory. In the contemporary, both complexes outperformed the control, showing the steadiness and stability throughout the

Table 4: Acute Toxicity Prediction.

Sl. No.	IP LD_{50} Log 10			IV LD_{50} Log 10			oral LD_{50} Log 10			SC LD_{50} Log 10		
	mmol/kg	mg/kg	Class	mmol/kg	mg/kg	Class	mmol/kg	mg/kg	Class	mmol/kg	Mg/kg	Class
1.	0,097 in AD	481,000 in AD	IV in AD	-0,847 in AD	54,680 in AD	IV in AD	0,455 in AD	1095,000 in AD	IV in AD	0,352 in AD	865,500 in AD	IV in AD
2.	0,193 in AD	630,500 in AD	V in AD	-0,687 in AD	83,090 in AD	IV in AD	0,300 in AD	807,500 in AD	IV in AD	0,686 out of AD	1964,000 out of AD	V out of AD
3.	0,528 in AD	871,500 in AD	V in AD	-0,795 in AD	41,430 in AD	IV in AD	0,586 in AD	996,500 in AD	IV in AD	0,328 in AD	549,100 in AD	IV in AD
4.	0,262 in AD	819,000 in AD	V in AD	-0,321 in AD	213,800 in AD	IV in AD	0,189 in AD	692,300 in AD	IV in AD	0,485 out of AD	1368,000 out of AD	V out of AD
5.	0,252 out of AD	551,300 out of AD	V out of AD	-0,058 in AD	270,100 in AD	IV in AD	0,805 in AD	1966,000 in AD	IV in AD	0,234 in AD	528,200 in AD	IV in AD
6.	0,634 in AD	1390,000 in AD	Non-toxic in AD	-0,687 in AD	83,760 in AD	IV in AD	0,337 in AD	700,900 in AD	IV in AD	0,486 in AD	988,300 in AD	V In AD
7.	0,135 in AD	502,800 in AD	V in AD	-0,217 in AD	223,700 in AD	IV in AD	0,263 in AD	675,500 in AD	IV in AD	0,819 in AD	2340,000 in AD	IV in AD
8.	0,271 in AD	602,300 in AD	V in AD	-0,281 in AD	168,800 in AD	IV in AD	0,786 in AD	1968,000 in AD	IV in AD	0,933 out of AD	2762,000 out of AD	V out of AD
9.	0,483 in AD	1150,000 in AD	V in AD	-0,427 in AD	141,600 in AD	IV in AD	0,733 in AD	2046,000 in AD	V in of AD	1,231 in AD	6441,000 in AD	NT Out Of AD
10.	0,175 out of AD	646,700 out of AD	V out of AD	-0,416 in AD	165,800 in AD	IV in AD	0,263 in AD	792,700 in AD	IV in AD	0,267 out of AD	800,000 out of AD	NT in AD
Control	-0,039 out of AD	527,800 out of AD	V out of AD	-1,150 in AD	40,930 in AD	IV in AD	0,164 in AD	841,700 in AD	IV in AD	0,518 out of AD	175,000 out of AD	IV Out Of AD

IP-Intraperitoneal route of administration, IV-Intravenous route of administration, Oral-Oral route of administration, SC-Subcutaneous route of administration, NT-Non-Toxic; Comma (,) is used as a decimal separator (e.g., 527,800=527.800).

Table 5: Predicted Adverse Reactions of Compounds.

Compounds	Pa/Pi	Hepatotoxicity	Arrhythmia	Myocardial infarction	Cardiac failure	Nephrotoxicity
1	Pa	0.773	0.571	0.287	0.24	NA
	Pi	0.07	0.061	0.233	0.231	NA
2	Pa	NA	NA	NA	NA	NA
	Pi	NA	NA	NA	NA	NA
3	Pa	0.665	0.428	0.535	0.478	NA
	Pi	0.114	0.164	0.038	0.067	NA
4	Pa	0.639	NA	NA	0.281	NA
	Pi	0.125	NA	NA	0.192	NA
5	Pa	0.774	0.366	0.629	0.705	0.379
	Pi	0.083	0.216	0.024	0.007	0.097
6	Pa	0.558	NA	0.579	0.61	NA
	Pi	0.165	NA	0.031	0.018	NA
7	Pa	NA	NA	0.337	0.258	NA
	Pi	NA	NA	0.133	0.213	NA
8	Pa	0.425	0.426	0.294	NA	NA
	Pi	0.241	0.165	0.213	NA	NA
9	Pa	NA	0.458	0.384	0.354	0.336
	Pi	NA	0.142	0.079	0.128	0.124
10	Pa	0.677	0.435	NA	NA	NA
	Pi	0.109	0.089	NA	NA	NA
Control		NA	NA	NA	NA	NA

simulation. Comparatively, complex 8 showed a range between 0.20-0.30 nm with some spikes reaching approx. 1.20 nm indicative of relatively stable binding. Similarly, compound 10 also demonstrated stable behavior maintained within 0.20-0.35 nm with limited fluctuations up to 1.10 nm, particularly during the later stage.

On the other hand, fluctuation analysis was performed through RMSF to evaluate the flexibility of the residues (Fatriansyah *et al*., 2022). Both compounds displayed lower values across residues, indicating rigidity of the protein. The major fluctuation was observed within 0.05-0.12 nm by compound 8, for compound 10, it maintained larger RMSF values within the range of 0.06-0.15 nm with minor peaks. Whereas the reference compound exhibited higher fluctuations across several regions throughout the simulation. A prominent peak was also noticed around 35-40 residues with average value 0.32-0.35 nm, demonstrating significant flexibility. The plots of RMSD and RMSF are given in Figure 2.

Solvent Accessible Surface Area

The SASA (Solvent Accessible Surface Area) was calculated to determine the conformation and protein folding changes that occurred throughout the simulation (Mukherjee *et al*., 2018). The reference compound showed significant fluctuations ranging between 12 and 18, indicating compactness instability. In contrast, both compounds maintained consistent SASA values. Compound 8 displayed lower SASA values, mainly fluctuating between 5 nm^2 and 8 $nm^{2,}$ indicating a more compact protein conformation with reduced solvation exposure. To some extent, compound 10 maintains values between approximately 2-6 nm^2, reflecting the highest degree of compactness represented in Figure 3A.

Solvation Free Energy Analysis

The solvation energy depicts changes in Gibbs free energy, which measures the energetic favorability of the interaction of the complexes. The lower values indicate stable solvation interaction (Huang *et al*., 2024). The values are plotted against a 100 ns simulation time depicted in Figure 3B. From the thorough analysis, the reference compound exhibited negative solvation values fluctuating between -15 and -25. However, it also showed noticeable fluctuations. For compound 8, it displayed moderate values ranging between -6 and 10, which remained stable across the entire simulation, indicating a stable conformation. For compound 10, the investigation highlights the fluctuation between -5 and -10 nm, showing almost the same as compound 8, indicating stable solvation behavior.

Radius of Gyration Determination

The Rg was analyzed to evaluate the compactness and overall structural stability of protein-ligand complexes, where lower values indicate more compactness and stability or protein conformation (Wang *et al.*, 2024). The reference compound showed steadiness at 2 nm, showing some minute peaks. Whereas both compounds showed lower values relative to the control compound, ranging between 1.3 and 1.4 nm. A slight peak was observed by compound 8 at 1.4 nm. Both compounds overlapped each other, indicating favorable stability (Figure 3C).

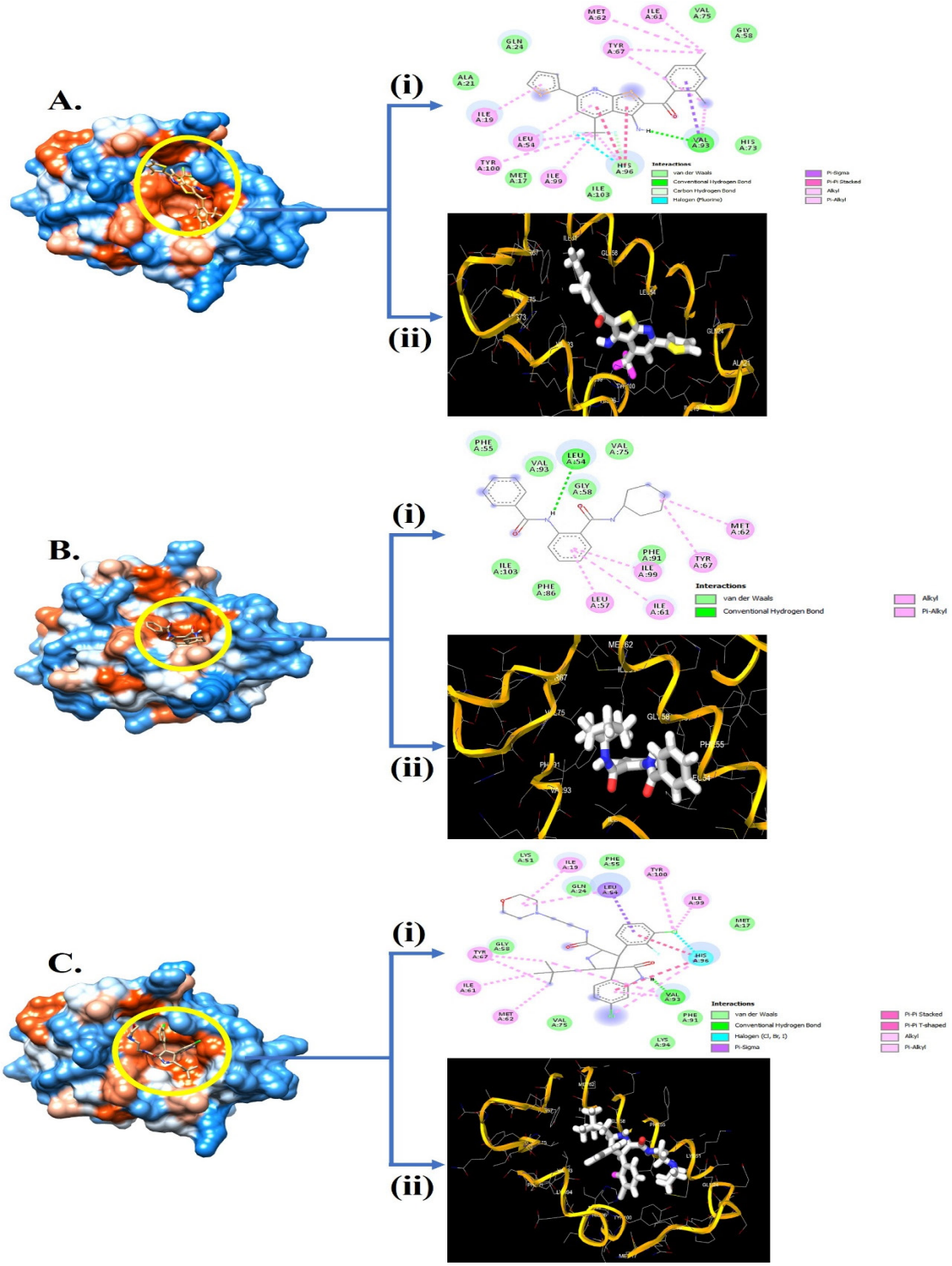

Figure 1: (A) Interacting Illustration of Compound 8 represented with different Poses, including surface pose, (i) 2-D interaction, and (ii) 3-D interaction. (B) Interacting Illustration of Compound 10 represented with different Poses, including surface pose, (i) 2-D interaction, and (ii) 3-D interaction. (C) Interacting Illustration of Reference Compound represented with different Poses, including surface pose (i) 2-D interaction, and (ii) 3-D interaction.

Table 6: Pharmacokinetics Profiling.

Sl. No.	water solubility	Caco2	HIA	Skin	BBB	CYP2D6	Clearance	Renal	AMES	Max Dose	hERG I	hERG II
1.	-5.351	1.246	92.073	-2.707	0.015	No	0.979	No	Yes	0.308	No	Yes
2.	-4.664	0.517	94.057	-2.675	-0.684	No	0.192	No	Yes	-0.138	No	Yes
3.	-6.273	1.611	97.575	-2.664	0.716	No	0.139	No	Yes	0.431	No	Yes
4.	-5.297	1.572	89.964	-3.026	0.184	No	0.034	No	No	0.253	No	Yes
5.	-4.326	1.296	95.726	-2.773	0.2	No	0.192	No	Yes	0.188	No	Yes
6.	-4.14	1.553	95.384	-2.735	0.124	No	0.091	No	No	-0.047	No	Yes
7.	-4.812	1.407	91.048	-3.031	0.215	No	0.128	No	No	0.333	No	No
8.	-4.37	1.361	92.317	-3.064	-0.032	No	0.178	No	No	-0.286	No	Yes
9.	-5.77	1.251	88.78	-2.715	0.119	No	0.004	No	Yes	0.42	No	Yes
10.	-6.859	1.256	89.378	-2.839	0.121	No	0.207	No	No	0.935	No	Yes
Ref	-4.027	0.993	95.343	-2.736	-0.835	No	0.538	No	No	-0.546	No	Yes

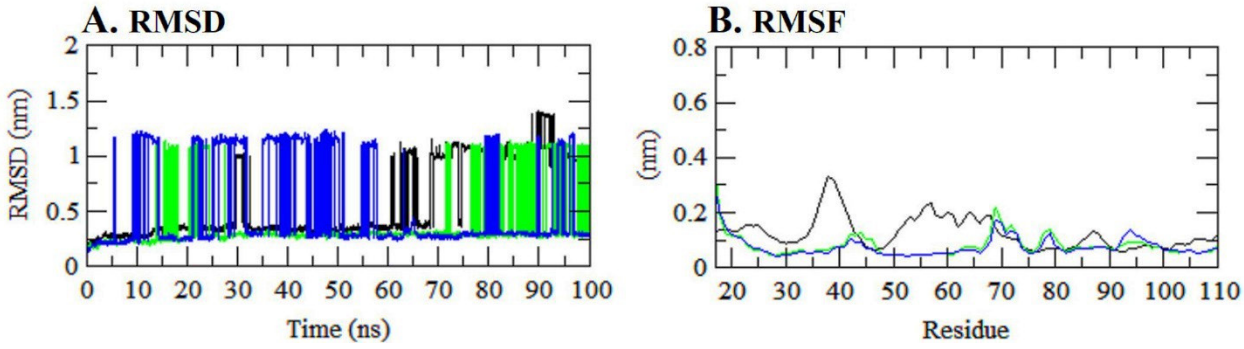

Figure 2: (A) RMSF and (B) RMSD plots throughout the simulation. Reference molecule is in black, blue color shows compound 8 and green shows compound 10.

Hydrogen Bonds Analysis

Hydrogen bonds play a vital role in simulation studies, often playing a role as anchors holding a drug in the preferred and correct orientation within the pocket. The HB (Hydrogen Bonds) plot (Figure 3D) represents higher variability in hydrogen bonding by the reference molecule. Peaks were observed at 3-4 bonds, particularly in the later stage of the trajectory, indicating less stability. The most consistent hydrogen bonding interactions were recorded for compound 8, typically maintained between 1 and 2 and increased to 3. However, 1-2 bonds are observed for compound 10 appears frequently less to compound 8.

DISCUSSION

Mouse Double Minute 2 is a critical E3 ubiquitin ligase that acts as a primary negative regulator of the p53 tumor suppressor. When the level of MDM2 increases, it likely blocks p53 activity, which is commonly found in several cancers occurred worldwide. The phenomenon makes MDM2 a hallmark for cancers (Lin *et al.*, 2024; Wang *et al.*, 2024). Therefore, the urgent need is to develop a potent small molecule that could terminate the upregulation effectively in silent wild-type p53. Looking for a small molecule that can disrupt the interaction is a vital strategy to restoring natural tumor suppressive function and inhibiting drug resistance. Our research was primarily focused on finding a small molecular inhibitor. This utilized a multi-stage computational approach to identify the best lead compound. The known inhibitor of MDM2, Mi-63, attached to the MDM2 protein, was taken as a reference molecule. Initially, the library screening and molecular docking interaction studies were performed within the Mcule platform. The screening resulted in 100 compounds, followed by Lipinski's rule. The docking energies recorded for the control compound were -7.8 kcal/mol. For refining of the compound's, screened compounds were checked for any structural toxicity by the Toxicity checker available in the Mcule platform. The structure-based toxic compounds were eliminated. Afterwards, further approaches were applied, such as biological activity prediction, cell lines prediction, LD_{50} predictions, possible side effects, and pharmacokinetics profiling (Tables 1-6).

The integrated analysis was compared carefully with the inhibitor compound. The analysis highlights two compounds, compound 8 with IUPAC 2-benzamido-N-cyclohexylbenzamide (MCULE-4592638188-0-189) and compound 10 (MCULE-8527570511) with IUPAC 3-amino-6-thiophen-2-yl-4-(trifluoromethyl)

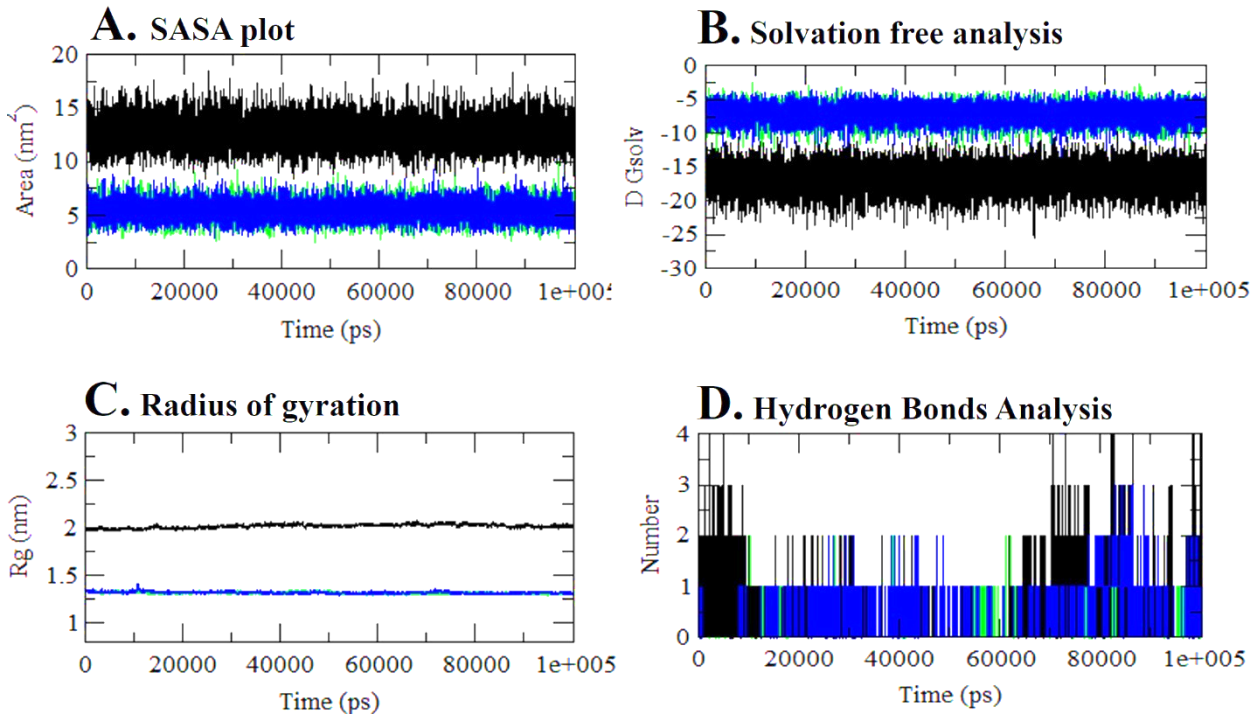

Figure 3: (A) SASA plot of the protein complex. (B) Solvation free energy analysis of the protein complex. (C) Radius of gyration plot (nm). (D) Hydrogen bond analysis. In all panels, black represents the reference compound, blue represents Compound 8, and green represents Compound 10.

thieno[2,3-b]pyridin-2-yl]-(2,4-dimethylphenyl)methanone respectively. These molecules revealed favorable results in all the parameters. The screening of PASS predictions revealed high specificity for STAT3 and HSP-27, which are linked to MDM2 stabilization and p53 suppression. Followed by CLC-pred analysis confirmed that these compounds possess targeted cytotoxicity potential against breast and lung cancer cell lines, such as MDA-MB. The LD_{50} result relies on classes IV and V, which are considered a safe profile supported by fewer possible side effects analyzed by AdverPred analysis compared to the control, exhibiting higher LD_{50} values. Moreover, drug likeness profiles demonstrated several supporting parameters, including $Caco_2$ permeability and low systemic clearance. The detailed analysis of the binding modes is visualized through 3D surface mapping, 2D diagram, and 3D diagram. On a favorable note, the interaction diagram revealed significant reliance on a conserved set of amino acid residues. The lead candidates and the control share critical interactions with VAL93, serving as the primary anchor. Compound 8 demonstrated a unique interaction with LEU54 via a conventional hydrogen bond, proving stable anchoring within the pocket. Also, there was a remarkable overlap in hydrophobic residues LEU54, ILE61, MET62, TYR67, VAL75, ILE99, and TYR100 that appear consistently forming deep hydrophobic cleft which were detected, which is essential for stabilization of the ligands. Residues like GLY 58, ALA21, and GLN24 in van der Waals interactions suggest a high degree of shape complementarity (Figures 1A-C). All these results worked as a supporting pillar in synthesizing the final lead candidate.

At last, the molecular dynamics studies were conducted at 100 ns, providing atomistic proof of the structural superiority of these compounds. Both compounds maintained highly stable trajectories. However, the hydrogen bonds were slightly lower than those of the reference compound. Comparatively, the study revealed through all analyses and post-simulation studies, compound MCULE-4592638188-0-189 has gained overall better results that can be considered as a promising lead inhibitor candidate.

Although we have performed multiple approach analyses, many possible research parameters can still be applied.

CONCLUSION

The study successfully identified the potent lead candidate for the targeted inhibition of the MDM2/p53/STAT3 signaling axis. By integrating multiple *in silico* approaches, we demonstrated that the compounds offer a superior balance of pharmacological efficacy and safety compared to conventional antineoplastic agents. Furthermore, an optimized pharmacokinetics profile highlights their potential against tumors. STAT3 and heat shock proteins offered a sophisticated strategy to overcome MDM2-mediated p53 silencing, particularly in lung and breast malignancies. Broad-spectrum cell lines were also observed to have high IAP and favorable activity and inactivity scores. The

compound also showed significantly higher binding energy, exhibiting minimal side effects. The higher structural stability and robustness observed in simulation trajectories provide strong evidence to maintain the inhibitory function under physiological conditions. The study was truly based on an *in silico* approach, and therefore experimental validations need to be checked to support the prediction in order to perform proper clinical trials of the identified drug and to seek reassurance before moving forward with practical use.

ACKNOWLEDGEMENT

The authors gratefully acknowledge the embryo genomics facility for providing valuable assistance and support in the bioinformatics analysis conducted in this study.

ABBREVIATIONS

MDM2: Murine double minute 2; **ER:** Estrogen receptor alpha; **MMP-9:** Matrix metalloproteinase-9; **ADMET:** Absorption, Distribution, Metabolism, Excretion, and Toxicity; **RMSD:** Root Mean Square Deviation, **RMSF:** Root Mean Square Fluctuation; **SASA:** Solvent Accessible Surface Area; **HB:** Hydrogen Bonds.

CONFLICT OF INTEREST

The authors declare that there is no conflict of interest.

SUMMARY

This study identified an auspicious lead compound targeting the MDM2/p53/STAT3 axis through an integrated *in silico* approach. The compound showed promising efficacy, safety, pharmacokinetics, binding affinity, and simulation stability, with potential activity against lung and breast cancers. However, experimental validation is still required before clinical application.

REFERENCES

Abuetabh, Y., Wu, H.-H., Chai, C., Al Yousef, H., Persad, S., Sergi, C. M., and Leng, R. (2022). DNA damage response revisited: The p53 family and its regulators provide endless cancer therapy opportunities. Experimental and Molecular Medicine, 54, 1658-1669.

Alsamghan, A. S., Alwabli, A. S., Abadi, M., Alsaleem, S. A., Anbari, D. M., Alomari, A. S., Alzahrani, O., Alam, Q., and Tarique, M. (2020). From sequence analysis of DPP-4 to molecular docking-based searching of its inhibitors. Bioinformation, 16(6), 444-451.

Berman, H. M. (2000). The Protein Data Bank. Nucleic Acids Research, 28, 235-242.

Bishwakarma, R. L., Jha, R. K., Choudhary, P., Shukla, A. K., Panwar, S., Kumar, A., and Kumari, A. (2026). Molecular insights for virtual screening of potential lead compounds of barley against infection of Helicobacter pylori. *In silico* Research in Biomedicine, 2, 100188.

Bhatia, N., Khator, R., Kulkarni, S., Singh, Y., Kumar, P., and Thareja, S. (2023). Recent advancements in the discovery of MDM2/MDM2-p53 interaction inhibitors for the treatment of cancer. Current Medicinal Chemistry, 30, 3668-3701.

Brown, A. L., Lian, X., and Wang, Q. (2026). The structure, pathogenesis, and inhibition of the p53-MDM2 pathway. Cancers, 18, 546.

Bultum, L. E., Tolossa, G. B., Kim, G., Kwon, O., and Lee, D. (2022). *In silico* activity and ADMET profiling of phytochemicals from Ethiopian indigenous aloes using pharmacophore models. Scientific Reports, 12, 22221.

Callis, J. (2014). The ubiquitination machinery of the ubiquitin system. The Arabidopsis Book, 12, e0174.

Camps-Fajol, C., Cavero, D., Minguillón, J., and Surrallés, J. (2025). Targeting protein-protein interactions in drug discovery: Modulators approved or in clinical trials for cancer treatment. Pharmacological Research, 211, 107544.

Cheng, M.-Y., Hsu, I.-C., Huang, S.-Y., Chuang, Y.-T., Ke, T.-Y., Chang, H.-W., Chu, T.-H., Chen, C.-Y., and Cheng, Y.-B. (2024). Marine prostanoids with cytotoxic activity from octocoral Clavularia spp. Marine Drugs, 22, 219.

Checler, F., Alves da Costa, C., Ancolio, K., Chevallier, N., Lopez-Perez, E., and Marambaud, P. (2000). Role of the proteasome in Alzheimer's disease. Biochimica et Biophysica Acta (BBA) - Molecular Basis of Disease, 1502, 133-138.

Choudhary, H. B., Mandlik, S. K., and Mandlik, D. S. (2023). Role of p53 suppression in the pathogenesis of hepatocellular carcinoma. World Journal of Gastrointestinal Pathophysiology, 14, 46-70.

Di Grazia, G., Conti, C., Nucera, S., Stella, S., Massimino, M., Giuliano, M., Schettini, F., Vigneri, P., and Martorana, F. (2025). Bridging the gap: The role of MDM2 inhibition in overcoming treatment resistance in breast cancer. Critical Reviews in Oncology/Hematology, 214, 104834.

Fatriansyah, J. F., Boanerges, A. G., Kurnianto, S. R., Pradana, A. F., Fadilah, and Surip, S. N. (2022). Molecular dynamics simulation of ligands from Anredera cordifolia (Binahong) to the main protease (Mpro) of SARS-CoV-2. Journal of Tropical Medicine, 2022, 1-13.

Gadaleta, D., Vuković, K., Toma, C., Lavado, G. J., Karmaus, A. L., Mansouri, K., Kleinstreuer, N. C., Benfenati, E., and Roncaglioni, A. (2019). SAR and QSAR modeling of a large collection of LD50 rat acute oral toxicity data. Journal of Cheminformatics, 11, 58.

Habara, M., and Shimada, M. (2022). Estrogen receptor α revised: Expression, structure, function, and stability. BioEssays, 44.

Hepowit, N. L., Kolbe, C., Zelle, S. R., Latz, E., and MacGurn, J. A. (2022). Regulation of ubiquitin and ubiquitin-like modifiers by phosphorylation. FEBS Journal, 289, 4797-4810.

Hernández Borrero, L. J., and El-Deiry, W. S. (2021). Tumor suppressor p53: Biology, signaling pathways, and therapeutic targeting. Biochimica et Biophysica Acta (BBA) - Reviews on Cancer, 1876, 188556.

Hou, H., Sun, D., and Zhang, X. (2019). The role of MDM2 amplification and overexpression in therapeutic resistance of malignant tumors. Cancer Cell International, 19, 216.

Huang, K., Duan, L., and Zhang, J. Z. H. (2024). From implicit to explicit: An interaction-reorganization approach to molecular solvation energy. Journal of Chemical Theory and Computation, 20, 10961-10971.

Ivanov, S. M., Lagunin, A. A., Rudik, A. V., Filimonov, D. A., and Poroikov, V. V. (2018). ADVERPred-Web service for prediction of adverse effects of drugs. Journal of Chemical Information and Modeling, 58, 8-11.

Khan, M. K. A., Ahmad, S., Rabbani, G., Shahab, U., and Khan, M. S. (2022). Target-based virtual screening, computational multiscoring docking and molecular dynamics simulation of small molecules as promising drug candidate affecting kinesin-like protein KIFC1. Cell Biochemistry and Function, 40, 451-472.

Kiss, R., Sandor, M., and Szalai, F. A. (2012). Mcule.com: A public web service for drug discovery. Journal of Cheminformatics, 4, P17.

Kung, C.-P., and Weber, J. D. (2022). It's getting complicated-A fresh look at p53-MDM2-ARF triangle in tumorigenesis and cancer therapy. Frontiers in Cell and Developmental Biology, 10.

Lagunin, A. A., Rudik, A. V., Pogodin, P. V., Savosina, P. I., Tarasova, O. A., Dmitriev, A. V., Ivanov, S. M., Biziukova, N. Y., Druzhilovskiy, D. S., Filimonov, D. A., *et al.* (2023). CLC-Pred 2.0: A freely available web application for *in silico* prediction of human cell line cytotoxicity and molecular mechanisms of action for druglike compounds. International Journal of Molecular Sciences, 24, 1689.

Lang, B. J., Guerrero-Giménez, M. E., Prince, T. L., Ackerman, A., Bonorino, C., and Calderwood, S. K. (2019). Heat shock proteins are essential components in transformation and tumor progression: Cancer cell intrinsic pathways and beyond. International Journal of Molecular Sciences, 20, 4507.

Lin, W., Yan, Y., Huang, Q., and Zheng, D. (2024). MDMX in cancer: A partner of p53 and a p53-independent effector. Biologics, 18, 61-78.

Liu, H., Zhou, X., Wang, H., Cao, F., and Han, W. (2025). Gaussian accelerated molecular dynamics simulations combined with NRIMD to explore the mechanism of substrate selectivity of Cid1 polymerase for different nucleoside triphosphates. International Journal of Molecular Sciences, 26, 9325.

Malik, A., Afaq, S., Gamal, B. E., Ellatif, M. A., Hassan, W. N., Dera, A., Noor, R., and Tarique, M. (2019). Molecular docking and pharmacokinetic evaluation of natural compounds as targeted inhibitors against Crz1 protein in Rhizoctonia solani. Bioinformation, 15(4), 277-286.

Maruyama, Y., Igarashi, R., Ushiku, Y., and Mitsutake, A. (2023). Analysis of protein folding simulation with moving root mean square deviation. Journal of Chemical Information and Modeling, 63, 1529-1541.

Mirabelli, P., Coppola, L., and Salvatore, M. (2019). Cancer cell lines are useful model systems for medical research. Cancers, 11, 1098.

Mukherjee, S., and Bahadur, R. P. (2018). An account of solvent accessibility in protein-RNA recognition. Scientific Reports, 8, 10546.

Muteeb, G., Rehman, M. T., AlAjmi, M. F., Aatif, M., Farhan, M., and Shafi, S. (2022). Identification of a potential inhibitor (MCULE-8777613195-0-12) of New Delhi metallo-β-lactamase-1 (NDM-1) using *in silico* and *in vitro* approaches. Molecules, 27, 5930.

Noumi, E., Snoussi, M., Bouali, N., Alshammari, M. M., Altayb, H. N., Afzal, M., and De Feo, V. (2025). Structure-based virtual screening, molecular docking, and MD simulation studies: An *in silico* approach for identifying potential MBL inhibitors. PLOS ONE, 20, e0324836.

Parasuraman, S. (2011). Prediction of activity spectra for substances. Journal of Pharmacology and Pharmacotherapeutics, 2(1), 52-53.

Patel, J. M., and Jeselsohn, R. M. (2022). Estrogen receptor alpha and ESR1 mutations in breast cancer (pp. 171-194).

Petersen, H. G. (1995). Accuracy and efficiency of the particle mesh Ewald method. Journal of Chemical Physics, 103, 3668-3679.

Pires, D. E. V., Blundell, T. L., and Ascher, D. B. (2015). pkCSM: Predicting small-molecule pharmacokinetic and toxicity properties using graph-based signatures. Journal of Medicinal Chemistry, 58, 4066-4072.

Psatha, K., Kollipara, L., Drakos, E., Deligianni, E., Brintakis, K., Patsouris, E., Sickmann, A., Rassidakis, G. Z., and Aivaliotis, M. (2023). Interruption of p53-MDM2 interaction by Nutlin-3a in human lymphoma cell models initiates a cell-dependent global effect on transcriptome and proteome level. Cancers, 15, 3903.

Rahmati, S., Zandi, F., Ahmadi, K., Adeli, A., Rastegarpanah, N., Amanlou, M., and Vaziri, B. (2025). Computational structure-based design of antiviral peptides as potential protein-protein interaction inhibitors of rabies virus phosphoprotein and human LC8. Heliyon, 11, e41520.

Roskoski, R. (2023). Rule of five violations among the FDA-approved small molecule protein kinase inhibitors. Pharmacological Research, 191, 106774.

Russano, F., Sturlese, M., Dall'Olmo, L., Callegarin, F., Brugnolo, D., Del Fiore, P., Patti, V., Purpura, A., Moro, S., Rastrelli, M., *et al.* (2025). MDM2 in tumor biology and cancer therapy: A review of current clinical trials. International Journal of Molecular Sciences, 27, 99.

Sadia, H., Qureshi, I. Z., Naveed, M., Aziz, T., Alharbi, M., Alasmari, A. F., and Albekairi, T. H. (2024). Natural AI-based drug designing by modification of ascorbic acid and curcumin to combat buprofezin toxicity by using molecular dynamics study. Scientific Reports, 14, 28445.

Sait, K. H. W., Alam, Q., Anfinan, N., Al-Ghamdi, O., Malik, A., Noor, R., Jahan, F., and Tarique, M. (2019). Structure-based virtual screening and molecular docking for the identification of potential novel EGFR kinase inhibitors against ovarian cancer. Bioinformation, 15(4), 287-294.

Saxena, G. (2019). Virtual screening, docking and molecular dynamics simulation of selected phytochemical compounds bound to receptor tyrosine kinases: A correlative anti angiogenic study. Bioinformation, 15, 613-620.

Sciot, R. (2021). MDM2 amplified sarcomas: A literature review. Diagnostics, 11, 496.

Shamloo, B., and Usluer, S. (2019). p21 in cancer research. Cancers, 11, 1178.

Subhasree, N., Jiangjiang, Q., Kalkunte, S., Minghai, W., and Ruiwen, Z. (2013). The MDM2-p53 pathway revisited. The Journal of Biomedical Research, 27, 254.

Sun, S. Y., and Crago, A. (2023). MDM2 implications for potential molecular pathogenic therapies of soft-tissue tumors. Journal of Clinical Medicine, 12, 3638.

Tecalco-Cruz, A. C., and Ramírez-Jarquín, J. O. (2017). Mechanisms that increase stability of estrogen receptor alpha in breast cancer. Clinical Breast Cancer, 17, 1-10.

Trott, O., and Olson, A. J. (2010). AutoDock Vina: Improving the speed and accuracy of docking with a new scoring function, efficient optimization, and multithreading. Journal of Computational Chemistry, 31, 455-461.

Vanommeslaeghe, K., Hatcher, E., Acharya, C., Kundu, S., Zhong, S., Shim, J., Darian, E., Guvench, O., Lopes, P., Vorobyov, I., *et al.* (2010). CHARMM general force field: A force field for drug-like molecules compatible with the CHARMM all-atom additive biological force fields. Journal of Computational Chemistry, 31, 671-690.

Wang, C., Chang, R., Li, J., and Li, L. (2024). TRIM47 silencing inhibits the malignant biological behaviors of prostate cancer cells by regulating MDM2/p53 signaling. Cell Biochemistry and Biophysics, 82, 1567-1578.

Wang, W., Albadari, N., Du, Y., Fowler, J. F., Sang, H. T., Xian, W., McKeon, F., Li, W., Zhou, J., and Zhang, R. (2024). MDM2 inhibitors for cancer therapy: The past, present, and future. Pharmacological Reviews, 76, 414-453.

Wang, Y., Zhou, Y., and Khan, F. I. (2024). Molecular insights into structural dynamics and binding interactions of selected inhibitors targeting SARS-CoV-2 main protease. International Journal of Molecular Sciences, 25, 13482.

Whiteley, A. E., Price, T. T., Cantelli, G., and Sipkins, D. A. (2021). Leukaemia: A model metastatic disease. Nature Reviews Cancer, 21, 46175.

Wolosowicz, M., Prokopiuk, S., and Kaminski, T. W. (2025). Matrix metalloproteinase-9 (MMP-9) as a therapeutic target: Insights into molecular pathways and clinical applications. Pharmaceutics, 17, 1425.

Yu, Q., Li, Y., Mu, K., Li, Z., Meng, Q., Wu, X., Wang, Y., and Li, L. (2014). Amplification of MDMX and overexpression of MDM2 contribute to mammary carcinogenesis by substituting for p53 mutations. Diagnostic Pathology, 9, 71.

Zakharov, A. V., Peach, M. L., Sitzmann, M., Filippov, I. V., McCartney, H. J., Smith, L. H., Pugliese, A., and Nicklaus, M. C. (2012). Computational tools and resources for metabolism-related property predictions. 2. Application to prediction of half-life time in human liver microsomes. Future Medicinal Chemistry, 4, 1933-1944.

Zhao, Y., Aguilar, A., Bernard, D., and Wang, S. (2015). Small-molecule inhibitors of the MDM2-p53 protein-protein interaction (MDM2 inhibitors) in clinical trials for cancer treatment. Journal of Medicinal Chemistry, 58, 1038-1052.

Zhu, I. Y., Lloyd, A., Critchley, W. R., Saikia, Q., Jade, D., Divan, A., Zeqiraj, E., Harrison, M. A., Brown, C. J., and Ponnambalam, S. (2025). Structure and function of MDM2 and MDM4 in health and disease. Biochemical Journal, 482, 241-262.

Zwickl, C. M., Graham, J. C., Jolly, R. A., Bassan, A., Ahlberg, E., Amberg, A., Anger, L. T., Beilke, L., Bellion, P., Brigo, A., *et al.* (2022). Principles and procedures for assessment of acute toxicity incorporating *in silico* methods. Computational Toxicology, 24, 100237.

Cite this article: Bakhsh T. Structure-Guided Virtual Screening and Molecular Dynamics Simulation of Selective Small-Molecule Inhibitors Targeting E3 Ubiquitin Ligase MDM2 in Breast Cancer. Int. J. Pharm. Investigation. 2026;16(4):1642-56.